Effect of shear rate on primary nucleation of para-amino benzoic acid in solution under different fluid dynamic conditions

Valentina Nappo[a], Rachel Sullivan[b], Roger Davey[c], Simon Kuhn[d], Asterios Gavriilidis[a], Luca Mazzei[a,*]

[a] University College London, Department of Chemical Engineering, Torrington Place, London, UK
[b] AstraZeneca, Pharmaceutical Development, Macclesfield, UK
[c] School of Chemical Engineering and Analytical Science, University of Manchester, Manchester, UK
[d] Department of Chemical Engineering, KU Leuven, Leuven, Belgium

ARTICLE INFO

ABSTRACT

The influence of shear rate on the primary nucleation of para-amino benzoic acid in water has been investigated via a series of cooling crystallization experiments. For each experiment, we recorded the induction time at various temperatures and supersaturation ratios, employing two flow devices: a capillary tube in which the solution was divided into hundreds of monodisperse droplets and a set of stirred vials. The capillary tube was used to perform experiments in stagnant conditions (motionless droplets) and low shear rate conditions (flowing droplets), while the stirred vials were used to perform experiments at relatively high shear rates. In this way, a wide range of shear rates was investigated. Comparing the results obtained for the motionless and flowing droplets, we saw that the nucleation rate is significantly increased (by several orders of magnitude) by the shear field; however, when the shear rate increases beyond a certain level (stirred vials experiments), we observed a drop in the nucleation rate. Thus, the results demonstrate a non-monotonic dependence of primary nucleation rate on shear rate. Various mechanisms to explain the effect of shear on nucleation are quantitatively and qualitatively discussed; however, at present no definitive conclusion can be drawn to identify the controlling mechanism.

1. Introduction

Cooling crystallization is extensively used by the pharmaceutical industry to produce and purify Active Pharmaceutical Ingredients (APIs). Crystallization consists essentially of two steps: nucleation, during which a new solid crystalline phase is formed from the liquid solution, and growth, during which solute molecules attach to the crystal nuclei increasing their size. Although the crystallization process has been known and used for decades, there is still a lack of fundamental knowledge about the nucleation mechanism, in particular under fluid dynamic conditions (Forsyth et al., 2016; Jawor-Baczynska et al., 2013). Evidence that mechanical perturbations in supersaturated solutions can trigger nucleation can be found from the beginning of the 20th century; however, systematic studies of the effect of fluid dynamics on nucleation kinetics only started in the 60s, when Mullin and Raven (1962) measured the metastable zone width (MZW) of a number of aqueous salt solutions as a function of the speed of the stirrer used to agitate them. Their results show that the MZW decreases as the agitation rate increases, reaches a minimum and then increases again. This non-monotonic behaviour was explained by the authors considering the combined effect of attrition and enhanced diffusion. More recently, Liu and Rasmuson (2013) and Liu et al. (2014, 2015) per-

formed a series of experiments to evaluate the effect of agitation on the primary nucleation rate of *m*-hydroxybenzoic acid and butyl paraben from organic solvents using various experimental systems such as traditional stirred crystallizers, small vials agitated with a magnetic stir bar and a Couette flow system. Their results show that the induction time strongly depends on the fluid dynamic conditions in the system; however, no definitive relation between shear rate and nucleation rate was found. Forsyth et al. (2015, 2016) performed similar experiments with the aim of correlating the induction time to the mean shear rate in laminar conditions; their results suggest that the induction time can be significantly reduced by increasing the shear rate.

To explain these results, different theories have been proposed. Among these, the most popular suggested in the literature and summarised by Liu and Rasmuson (2013) are the following: shear-induced molecular alignment, enhanced mass transfer, secondary nucleation, and agitation-enhanced cluster aggregation. Liu and Rasmuson (2013) discard the first two hypotheses on the basis that solute molecules are too small to be involved in molecular alignment (Gray et al., 1995) or enhanced mass transfer phenomena. For a long time, secondary nucleation has been considered responsible for the apparent reduction of the MZW; however, while it is widely accepted that secondary nucleation reduces the time lapse between the formation of the first nucleus and the moment in which it becomes visible, it is unlikely to be the dominating mechanism. Indeed, the induction time, defined as the time lapse between the creation of supersaturation and the formation of the first stable nucleus, is usually much longer than the additional time required to detect the nucleation event. Recently, a number of studies (Jawor-Baczynska et al., 2015, 2013; Penkova et al., 2006) have supported the enhanced cluster aggregation theory, which asserts that agitation promotes the aggregation of meso-scale clusters into larger stable clusters, so that nucleation proceeds through a two-step mechanism.

Despite the number of studies, the exact mechanism controlling nucleation under fluid dynamic conditions is still unclear. One reason for the poor understanding of the problem is that, traditionally, experiments are performed in large batch crystallizers, often characterised by complex fluid dynamics and non-homogeneous temperature.

In the last decades, there has been an increasing interest in microfluidic devices, as they represent effective tools to investigate crystal nucleation kinetics in well-controlled conditions (Leng and Salmon, 2009; Rossi et al., 2015). In particular, thanks to their unique characteristics, microfluidic devices allow fundamental studies to be performed on the nucleation mechanism using the *double pulse* method, which is based on the separation of the nucleation and growth stages (Galkin and Vekilov, 1999). This is achieved by keeping the solution at high supersaturation for a certain time (*nucleation time*) and then by rapidly lowering the supersaturation ratio, thereby making the solution quickly enter the so-called metastable zone. The supersaturation level in the metastable zone is too low to allow further nucleation, but is high enough to permit the growth of the nuclei already formed. This technique has been successfully used to study the nucleation rate of APIs and organic molecules in microfluidic devices (Laval et al., 2009; Lu et al., 2015; Teychené and Biscans, 2012). One reason for the success of microfluidic devices in kinetic studies is that, thanks to their small dimensions, it is easy to achieve temperature and concentration uniformity, even without the help of a stirrer; in addition, it is possible to change the fluid temperature, and therefore the supersaturation, far more rapidly than in large-scale systems. Despite these advantages, microfluidic chips are usually very expensive, their fabrication requiring costly equipment and trained personnel. In addition, they have a fixed geometry, which cannot be modified once the chip is sealed. In contrast, transparent polymeric capillaries offer more flexibility than conventional silicon or PDMS chips.

In this work, we compare nucleation rates of para-amino benzoic acid (PABA) in water obtained in three different fluid dynamic conditions: quiescent-stagnant conditions, low-shear laminar flow and high-shear turbulent flow. To achieve these fluid dynamic conditions, we performed experiments using two fluid flow devices: a capillary tube and a set of stirred vials. Quiescent and low-shear rate experiments were performed using a transparent PTFE capillary and applying the so-called *droplet method* in conjunction with the *double pulse technique*.

The *droplet method* consists in generating hundreds of small droplets of the crystallizing solution with the help of a carrier phase (in this case heptane); the *double pulse* temperature profile is then applied to the droplet array to separate the nucleation and growth stages. For the *quiescent conditions* experiments the droplets are kept motionless inside the channel, while for the *flowing conditions* low-shear experiments, the droplets are forced to move inside the channel at constant velocity, hence producing a gentle shear field. This approach has been previously used by Rossi et al. (2015), who observed that the recirculation inside the droplets slightly increased the crystal formation rate of adipic acid in water in a small range of supersaturation ratio values. The high-shear rate experiments are performed using a commercial stirred multiple reactor system (Crystal16). The above mentioned flow devices allow investigating a wide range of shear rates and can help to unveil the role of fluid dynamics in the nucleation of small molecules.

2.   Methodology

Although it is well known that nucleation is a stochastic process, for large enough volumes it can be described using deterministic models. This is the case for industrial and most laboratory-scale batch crystallizers. However, this is not true when the crystallizing volume is very small (typically <1 ml), as in droplets and small vials; in this case, nucleation appears as stochastic and must be described in statistical terms.

The experimental method used in this work consists in dividing the solution into a large number of small independent volumes. In such small volumes, nucleation is a stochastic process and can be modelled using the Poisson distribution (Jiang and Ter Horst, 2011; Rossi et al., 2015), where the probability P_T that at least one stable nucleus forms in a volume V during a time t_i at a certain supersaturation level is given by:

$$P_T\left(t_i, V, S\right) = 1 - \exp\left[-JV\left(t_n - t_g\right)\right] \tag{1}$$

where P_T is the probability, J is the deterministic nucleation rate, V is the solution volume, t_i is the induction time, t_g is the growth time, t_n is the *nucleation time* and S is the supersaturation ratio, defined as the ratio between the actual and the equilibrium concentrations of the solution (c/c_e). It is worth noticing that t_i, that is, the time needed to form the first stable nucleus under the specific experimental conditions, is an intrinsic property of the system and therefore depends only on the supersaturation level and the specific system investigated, while t_g and t_n depend on the equipment used and the experimentalist. In particular, t_g is the time needed by the nuclei to reach a detectable size, while t_n represents the time lapse between the moment the desired supersaturation is achieved and the moment in which one is able to detect the first crystal. Thus, it is:

$$t_n = t_i + t_g \tag{2}$$

It is worth noting that the probability P_T tends to unity for infinite volumes. When P_T approaches unity (for a given value of t_i, this occurs when V is a few multiples of $1/Jt_i$), the nucleation process can be treated as deterministic and volume-independent.

Experimentally, we can calculate the probability distribution as the fraction of droplets that contain at least one crystal after a time t_n (for a given growth time t_g):

$$P_E\left(t_i, V, S\right) = \frac{M^+\left[t_n\left(t_i\right), V, S\right]}{M} \tag{3}$$

where P_E is the experimental probability, M is the total number of solution volumes considered and M^+ is the number of solution volumes containing at least one crystal. By fitting the experimental data (3) with the theoretical distribution (1), we can estimate the value of the nucleation rate for each value of the supersaturation ratio. The method described above has been used both for the experiments performed using the capillary tube and the set of vials.

3. Experimental section

3.1. Materials

Para-amino benzoic acid (PABA) was purchased from Sigma Aldrich in powder form and used without further purification (H_2N-$C_6H_4CO_2H$, 99% pure). PABA has two well-known enantiotropic polymorphic forms, α and β. The transition temperature between the two forms has not been clearly identified in the literature: Gracin and Rasmuson (2004) observed the polymorphic transformation at 25 °C, but in a recent work by Hao et al. (2012) it was observed at 13.8 °C. The polymorphs can be easily identified using a standard optical microscope owing to their shape: the α-polymorph crystallises as long needles and it is the commercially available polymorph, while the β-polymorph crystallises in a prism shape (Gracin and Rasmuson, 2004). PABA can be crystallized from water as well as from a number of organic solvents (e.g. acetonitrile, 2-propanol, ethyl acetate, methanol, ethanol etc.) (Sullivan et al., 2014); however, it is reported that the β-form can be crystallized only from water and ethyl acetate (Gracin et al., 2005). Aqueous solutions of PABA were prepared using filtered deionized water (filter pore size 0.2 μm, conductivity <0.2 μS/cm). The solubility of PABA in water was taken from the experimental data of Gracin and Rasmuson (2004). Heptane ($CH_3(CH_2)_5CH_3$, Sigma Aldrich, anhydrous, 99% pure) was used, without further purification, as carrier phase for droplets formation in the capillary tube.

3.2. Experimental setup and procedure

To study the primary nucleation kinetics of PABA in water under stagnant and flowing conditions in the capillary tube, we used the *droplet method*, briefly described above. A PABA aqueous solution saturated at 27 °C was prepared by dissolving 0.5744 g of PABA in 100 ml of filtered deionised water; the solution was kept at about 50 °C for several hours to ensure the complete dissolution of the material. After that, monodisperse droplets were generated and stored into a long PTFE tube (IDEX, I.D. 1 mm, O.D. 1.58 mm, 4 m) by delivering the solution and the carrier phase (heptane) through a PEEK T-junction (IDEX, I.D. 0.5 mm) with the aid of syringe pumps (Harvard, PHD 2000 programmable). The T-junction allows the creation of a segmented pattern in which the droplets of the crystallising solution were kept separated by the carrier phase. Due to the hydrophobic nature of the tube, the heptane forms a thin liquid layer around the aqueous droplets preventing them from touching the channel walls. The absence of solid surfaces in contact with the crystallizing solution is beneficial as it decreases the chances of heterogeneous nucleation; in addition, it prevents clogging of the channel that can be caused by crystals growing on the tube walls during the experiments in flow conditions (moving droplets) (Poe et al.,
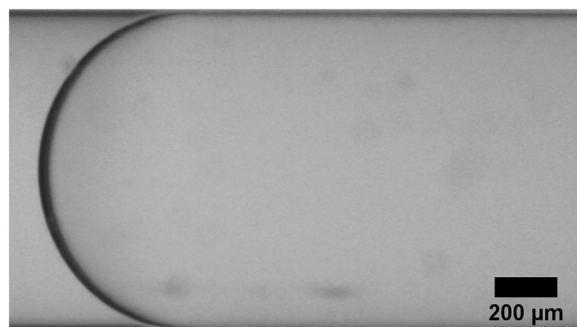
Fig. 1 – Water droplet in a 1 mm I.D. PTFE channel (heptane carrier phase).

2006). Due to the channel wettability and the fluid properties, the water droplets assume the characteristic capsular shape (Fig. 1).

Fig. 2 shows the schematic of the experimental setup. The droplets are generated within a Perspex enclosure which is kept above the saturation temperature ($T_1 > T_{sat}$) in order to prevent crystallization. For the experiments under *stagnant conditions*, after the droplets had filled the whole length of the tube, both ends of it were sealed and the tube was then immersed into a water bath at T_n (*nucleation section*). The time t_n during which the droplets were kept in the *nucleation section* was fixed a priori. After that, the droplet array was manually moved into the *growth section* at T_g for an additional time t_{GE}. Temperature has a strong influence on crystallization, and so its precise control is crucial in the investigation of the kinetics of the process. In these experiments, the temperature in the *nucleation* and *growth sections* was kept constant using two water baths (Huber, MPC-K6), while in the *droplet generation section* a fan heater kept the temperature above the saturation level.

Fig. 3 qualitatively shows the temperature profile used in the experiments. The temperature (T_g) of the *growth stage* was carefully chosen to be within the metastable zone in order to allow the growth of the nuclei formed during t_n while preventing further nucleation or dissolution. The reason is that, after the *nucleation stage*, the droplets might contain crystals that are too small to be detected. Therefore, in order to correctly estimate the number of droplets in which at least one stable nucleus has formed during the *induction time*, we let the nuclei grow until they reached a detectable size. This allows us to achieve the separation of nucleation and growth, and so to set t_g to zero in Eq. (1); so, for our specific experimental procedure, $t_n = t_i$.

To ensure that at the selected growth temperature the system was within the metastable zone, we placed the PTFE tubing containing the droplets directly in the growth stage for a time longer than the *experimental growth time* t_{GE} and we verified that no crystals were present in the droplets after this time. t_{GE} should be long enough that its value does not affect the outcome of the experiments. After a range of *experimental growth times* was investigated, we set the value of t_{GE} to be at least twice as large as the value of the *nucleation time* t_n.

After the set *experimental growth time* had elapsed, we observed the droplets using an optical microscope (Olympus IX50) and we counted the number of droplets containing at least one crystal. This procedure was used to determine the experimental probability distribution of *induction times* $P_E(t_i, V, S)$, as defined in Eq. (3). Polymorphs were identified by visual inspection only (Fig. 4).
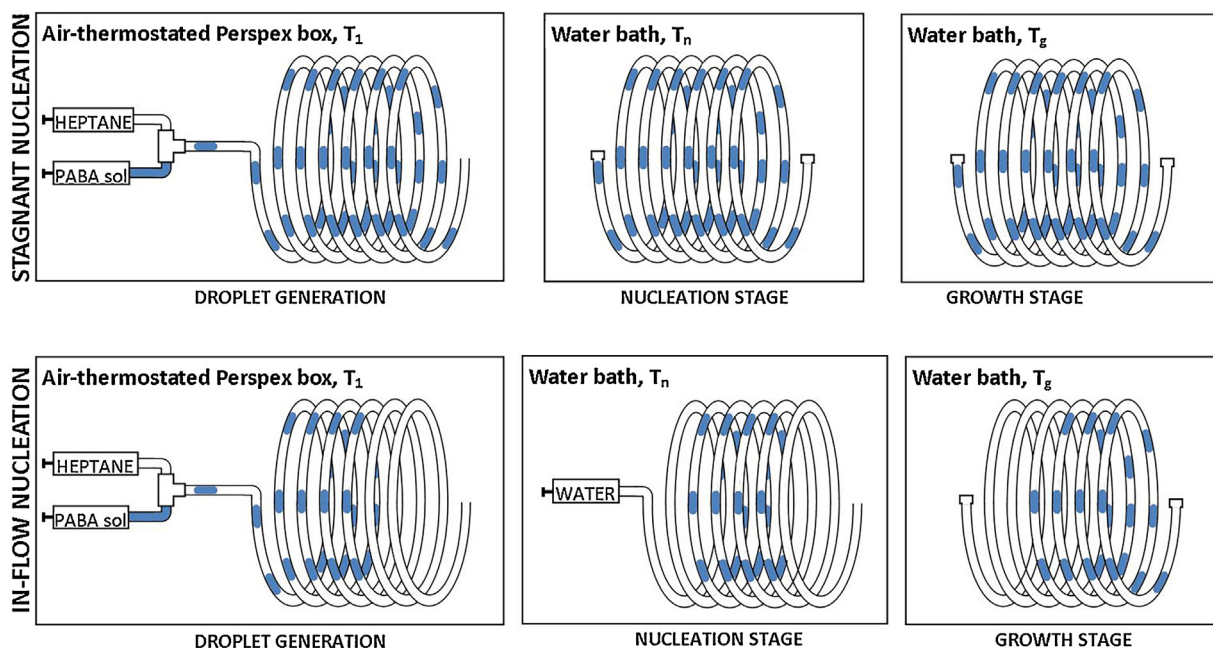
Fig. 2 – Schematic of the experimental setup used for the quiescent-conditions (stagnant nucleation) and flowing-conditions (in-flow nucleation) experiments.
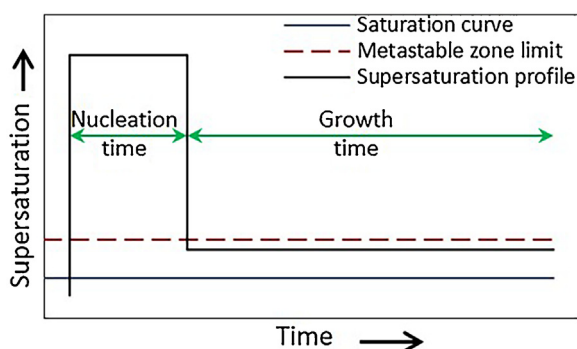
Fig. 3 – Qualitative representation of the supersaturation ratio profile used.

We connected a digital camera (Leica EC3) to the microscope to take pictures of the droplets. The pictures were then analysed using a Matlab® customised routine that calculates the volume of each droplet as the volume of the solid of revolution obtained by rotating the curve representing the droplet boundary about the horizontal axis. The script also calculated the mean and standard deviation of the droplet volume distribution for each experiment. It should be noted that, for the volume calculation, it was assumed that each droplet is axisymmetric along the horizontal direction.

To apply Eq. (1) correctly it is crucial that the droplets be monodisperse so that they can be considered to have the same volume. The polydispersity index (PDI) gives an indication about size uniformity and is defined as:

$$PDI = \frac{\sigma_V}{\tilde{V}} \qquad (4)$$

where σ_V is the standard deviation of the volume distribution and $\tilde{V}$ is the average droplet volume in each run. In each experiment, about 400 droplets were analysed and the PDI was below 5%; so we assumed that the droplets could be regarded as monodisperse (Castro-Hernández et al., 2011).

The microscope used for the crystal count was set in a laboratory where the temperature was about 23 °C. As this temperature was equal to the one chosen for the *growth stage* and the time needed for the crystal count was much shorter than the set *nucleation time*, it was assumed that no nucleation or dissolution occurred while counting the number of droplets containing PABA crystals. This was verified by counting again the percentage of droplets containing crystals after leaving the PTFE tube containing the droplets in the room for several hours without any temperature control. As the percentage stayed the same, we concluded that the outcome of the experiment was not affected by the experimental procedure.

A very similar procedure was used for the experiments in *flowing conditions* (moving droplets). After the droplet array had been generated in the Perspex box at $T_1 > T_{sat}$, the PTFE tube was connected to a glass syringe containing only DI water, the syringe was placed in the syringe pump, while the tube was immersed into the water bath at T_n. Immediately after placing the tube into the water bath, the syringe pump was activated (the flow rate was set at 100 µl/min for all the experiments) and the droplets started moving inside the tube. After the nucleation time had elapsed, the pump was stopped and both ends of the tube were immediately sealed; then, the droplet array was moved into the growth section, where it was left for a time equal to t_{GE}. Finally the tube was removed from the water bath and we observed the droplets under the microscope as described above for the *stagnant conditions* experiments and the experimental probability $P_E(t_i,V,S)$ was calculated. Each experiment was repeated three times to ensure reproducibility and the mean values and standard deviations were calculated.

For the experiments performed in the stirred vials, we used a commercial stirred multiple reactor system (Crystal16®). This consisted of a platform with an integrated heating/cooling system that can hold up to 16 small vials (of about 2 ml). The device was equipped with a turbidity sensor to register the onset of crystallization. Using this apparatus, the nucleation time t_n for a 0.8 ml PABA aqueous solution was
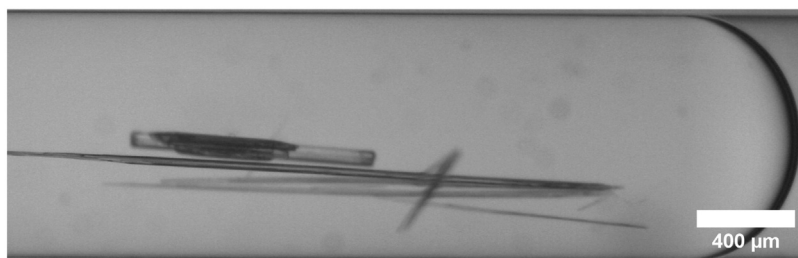
Fig. 4 – Aqueous droplets containing α-PABA crystals.

Table 1 – Summary of the experimental parameters for the *stagnant* and *flowing* conditions experiments in the microfluidic device and for the experiments in the stirred vials.

	Quiescent droplets	Flowing droplets	Stirred vials
T_n	3.0, 4.0, 5.0 °C	3.0, 5.0, 8.3 °C	20 °C
T_g	23 °C	23 °C	N/A
t_n	22–169 h	3–23 min	10–60 min
t_{GE}	0–888 h	0–888 h	N/A
S	2.29, 2.37, 2.47	2.02, 2.29, 2.47	1.67, 1.73, 1.8, 1.9, 1.97, 2.02
Volume	4 μl	4 μl	0.8 ml
Droplets velocity	0	2.12 mm/s	N/A
Stirring speed	N/A	N/A	1250 rpm

measured at various supersaturation ratios. Concentration and temperature uniformity was ensured by stirring the solution with a magnetic stirrer (1250 rpm). Because the solution volume in each vial is very small, the experimental nucleation rate is also considered to follow a Poisson distribution; therefore, the results were fitted with Eq. (1). For these experiments, the vials containing the solution were kept at 50 °C for 60 min to ensure complete dissolution of the crystals. Subsequently, the temperature was dropped to reach the desired supersaturation and the time corresponding to the onset of crystallization was recorded. This time corresponds to t_n in Eq. (1). Because in this case, unlike the experiments performed in the capillary tube, the nucleation time is recorded from the experiment rather than set a priori, the separation of nucleation and growth stage is not achieved ($t_n \neq t_i$) and the time the crystal nuclei need to reach a detectable size is not distinguishable from the actual nucleation time. As a consequence, t_g in Eq. (1) remains undetermined and was estimated as the shortest induction time measured, for each supersaturation level. Alternatively, t_g could be calculated based on the growth rate kinetics or estimated as a model parameter. However, Xiao et al. (2017) demonstrated that the three methods produce equivalent results in terms of nucleation rate. Therefore, we decided to take t_g as the shortest experimental induction time.

Table 1 summarises the experimental conditions used in this work for both the experimental setups described above. The detailed experimental procedure and setup for the experiments performed in the stirred vials can be found in Sullivan (2015). Although PABA crystallizes in two polymorphic forms (α and β), in all our experiments only the α-polymorph was obtained, and so all the results presented in this work relate to the α-polymorph.

4. Results and discussion

4.1. Nucleation rate under stagnant and flow conditions

Fig. 5(A–C) shows the probability function $P_E(t_i, V, S)$ obtained experimentally versus the *nucleation time* at different supersaturation ratios (2.29, 2.37, 2.47) in *stagnant* conditions (static droplets). As expected, with the increase of supersaturation level, the time needed to reach a certain value of the probability $P_E(t_i, V, S)$ decreases. Fig. 5(D) summarises the results obtained in term of nucleation rate. In particular, we found that the nucleation rate increases with the increase of the supersaturation ratio.

Fig. 6(A–C) shows the probability function $P_E(t_i, V, S)$ obtained experimentally versus the nucleation time under *flowing conditions* (moving droplets) at various supersaturation ratios (2.02, 2.29, 2.47). As in the previous case (*stagnant conditions* experiments), the probability of nucleation increased with the increase of nucleation time. However, the time needed for the probability to reach unity was orders of magnitude lower than in the previous case. This result corresponds to a much higher (deterministic) nucleation rate. Indeed, by fitting the experimental results with Eq. (1), we obtain values of the nucleation rate about two orders of magnitude higher than the values obtained in stagnant conditions at similar values of the supersaturation ratio (Fig. 6D). This suggests that the flow plays a crucial role in enhancing the nucleation rate. However, the mechanism behind this effect is still unclear in the scientific community. In the literature, it is suggested that the shear rate may be responsible for this enhancement, as it can increase the aggregation frequency of meso-scale clusters in solution (Liu and Rasmuson, 2013). This theory is based on the fact that the fluid flow is unlikely to enhance the probability of collision of single solute molecules; however, the velocity gradients generated in laminar flow may significantly increase the probability of collision of the larger meso-scale clusters. The existence of a significant number of meso-scale clusters in supersaturated solutions is not universally accepted by the scientific community, as it contradicts one fundamental assumption of the Classical Nucleation Theory (CNT), namely, that nuclei formation proceeds through a process of addition and subtraction of single solute molecules to a sub-critical size cluster. However, recent papers have brought more experimental evidence to support the existence of meso-scale clusters in protein crystallization (Chattopadhyay et al., 2005; Jawor-Baczynska et al., 2015, 2013; Pan et al., 2010); no evidence, nevertheless, has been found so far for the case of PABA crystals.

In single-phase laminar flow the shear rate experienced by these meso-scale clusters would be proportional to the average velocity in the channel:
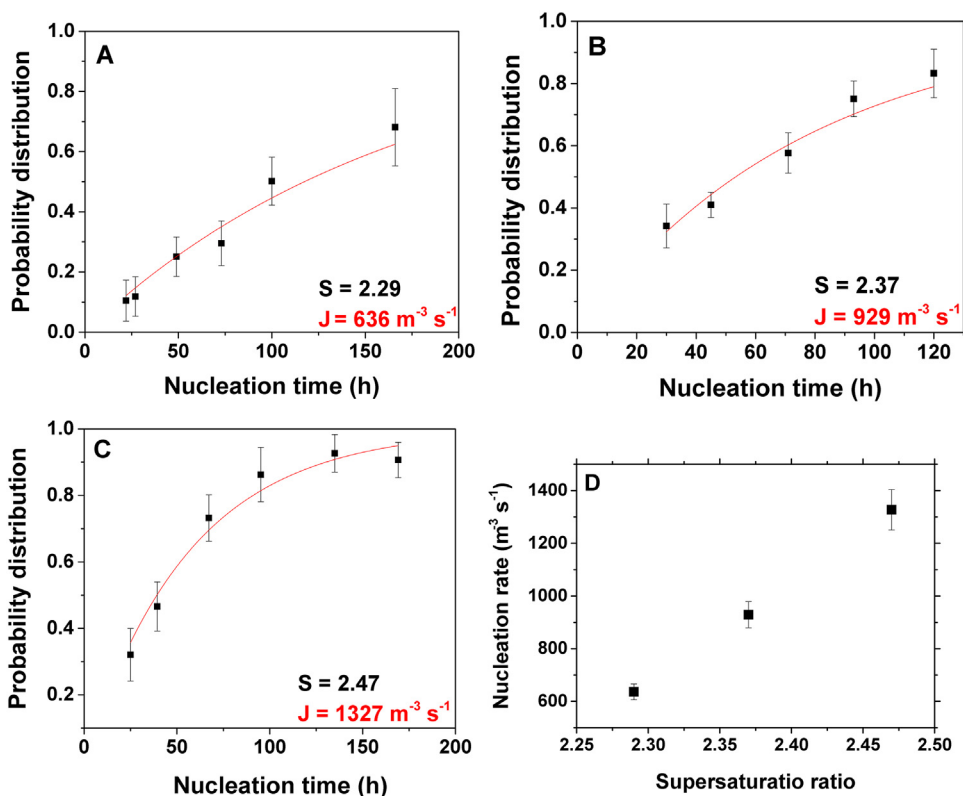
Fig. 5 – Experimental probability $P_E(t_n, V, S)$ versus nucleation time t_n of α-PABA in stagnant conditions at different supersaturation ratios: 2.29 (A), 2.37 (B), 2.47 (C); (D) nucleation rate J determined by fitting the experimental data with Eq. (1).
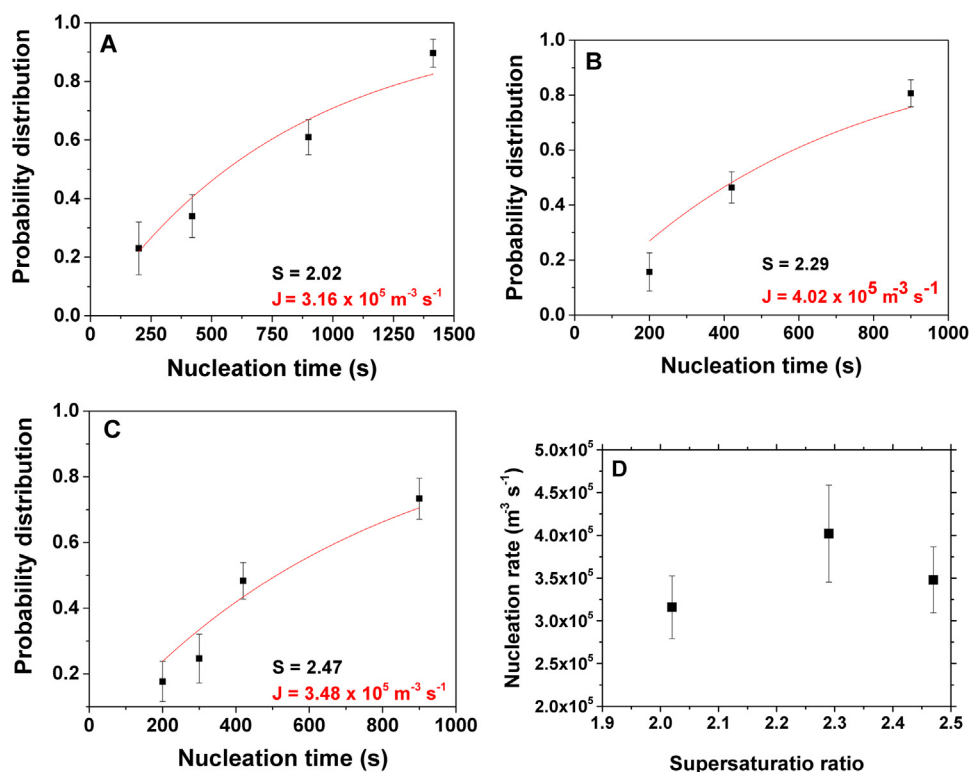
Fig. 6 – Experimental probability $P_E(t_n, V, S)$ versus nucleation time t_n of α-PABA in flowing conditions (moving droplets) at different supersaturation ratios 2.02 (A), 2.29 (B), 2.47(C); (D) nucleation rate J determined by fitting the experimental data with Eq. (1).

$$\dot{\gamma} \sim \frac{v_{av}}{R} \qquad (5)$$

where $\dot{\gamma}$ is the shear rate, v_{av} is the average velocity inside the channel and R is the channel radius.

Flow in micro and milli channels is normally characterised by very low Reynolds numbers (in the order of 10^0–10^1), and so no turbulence is present in these systems. For the *flowing conditions* experiments presented here, the Reynolds number
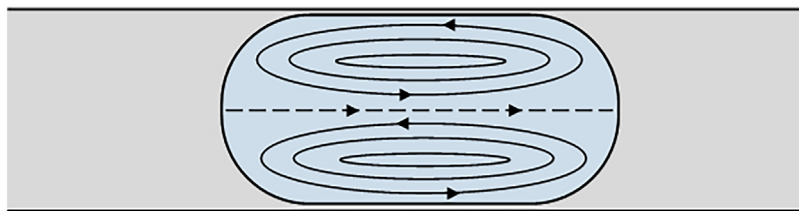
Fig. 7 – Schematic representation of recirculation patterns inside the droplet.

has unit order of magnitude, and so we can assume that the fluid flow is fully laminar. Because of the segmented flow configuration used in this work, two counter-rotating vortices are generated inside the droplets as qualitatively represented in Fig. 7. It can be shown that at the centre of the droplets (far from the front and the tail of the droplet) a fully developed parabolic velocity profile is established with the maximum velocity being twice the average mixture velocity (calculated as the ratio between the flow rate and the channel cross section) (Dore et al., 2012; Kurup and Basu, 2012). Although Eq. (5) does not strictly apply to two-phase segmented flow, in the light of the above considerations, it can be used to estimate the order of magnitude of the shear rate in the flowing droplets. In particular, considering the flow velocity and the channel dimensions used here, we obtain:

$$\dot{\gamma} \sim \frac{v_{av}}{R} = 4.2\,\text{s}^{-1} \tag{6}$$

Although this value might seem relatively small, the results obtained suggest that even a gentle shear field plays an important role in enhancing the nucleation rate.

It is also worth noting that our experimental results show that the supersaturation level does not seem to affect the results in the range analysed, because the differences between the nucleation rate values found at different supersaturation ratios are within the experimental error and no clear trend can be identified. For this reason, we consider that, for the present experimental conditions, the value of the nucleation rate is the same within the range analysed, regardless of mixture supersaturation. This is a surprising result and suggests that the effect of shear rate over nucleation overpowers the effect of supersaturation ratio in the range analysed.

4.2. Nucleation rate in stirred vials

Fig. 8 shows the nucleation rate obtained in the stirred vials by fitting the experimental results with Eq. (1). It can be noticed that nucleation rate in this case is within an order of magnitude of that obtained from the in-flow experiments for comparable supersaturation ratios.

The fluid dynamic conditions inside the vials are quite complex; so, an accurate assessment of the shear rate can be challenging. However, using a semi-empirical approach the average shear rate in stirred vessels can be expressed as a function of the specific energy dissipation rate (Pérez et al., 2006):

$$\dot{\gamma}_{av} = \left(\frac{P}{\mu V}\right)^{1/2} \tag{7}$$

where μ and V are the fluid viscosity and volume, respectively, and P is the power input, defined as (Coulson and Richardson, 1990):
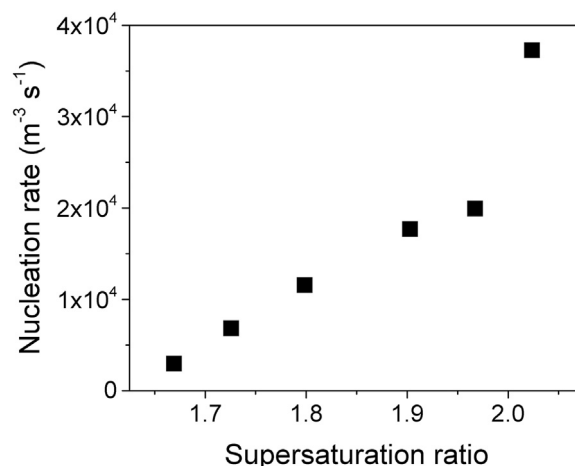
Fig. 8 – Experimental (deterministic) nucleation rates (J) obtained for α-PABA in water versus supersaturation ratio in stirred vials; each experimental point is based on 80 nucleation time measurements; the fluid dynamic conditions are the same for all the experiments. Adapted from Sullivan, (2015).

$$P = N_P \rho N^3 b \tag{8}$$

where ρ is the fluid density, N is the stirring rate, b is the length of the stir bar and N_P is the power number, which is characteristic of the impeller and tank geometry and stirring rate. Using the correlation of Furukawa et al. (2012) for unbaffled vessels to calculate N_P for our specific system, the average shear rate was calculated to be $\dot{\gamma}_{av} \approx 150\,\text{s}^{-1}$. This is about two orders of magnitude larger than the shear rate in the droplets flowing in the capillary.

The experimental results relative to the nucleation rate of α-PABA obtained both in the capillary system and in the stirred vials setup for selected values of the supersaturation ratio are summarised in Fig. 9. These specific nucleation rate values have been chosen with the intent of comparing the performances of the different systems presented here. Although the nucleation rate related to the stagnant conditions corresponded to a slightly higher supersaturation ratio we believe that our discussion does not lose generality as we are only interested in an order of magnitude comparison.

The nucleation rate was lowest under stagnant conditions in the capillary system, while it was highest in the flowing conditions experiments conducted at relatively low shear rate. The large difference (about two orders of magnitude) between the nucleation rates values found in these two conditions is even more significant considering that the stagnant conditions nucleation rate refers to slightly higher supersaturation values. These findings confirm that fluid dynamics plays a fundamental role in the nucleation process and lowers the time required for the formation of the first crystal in the supersaturated solution. Because this experimental method measures
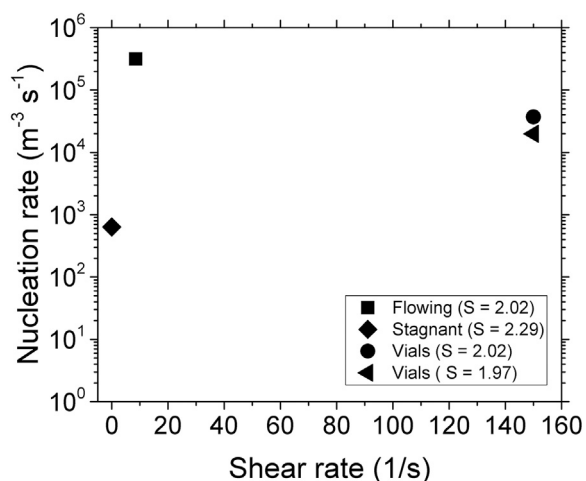
Fig. 9 – **Nucleation rate of α-PABA estimated from the best fit of Eq. (1) vs shear rate; the reported values refer to the microfluidic setup in stagnant conditions (S = 2.29) and flowing conditions (S = 2.02) and to the stirred vials (S = 1.97, 2.02).**

primary nucleation rates, this effect cannot be attributed to the enhancement of secondary nucleation. On the basis of previous studies, we can argue that the reduction of induction time is due to the enhancement of the rate of collision of meso-scale clusters promoted by the motion of the fluid. However, this cannot be confirmed without further experimentation that might unveil the presence of large meso-scale clusters in the supersaturated solution, which is at the base of the two-step nucleation theory.

For the stirred vials experiments, although the average shear rate is about two orders of magnitude larger than in the flowing conditions experiments, the nucleation rate found is about one order of magnitude lower. This result may be explained considering the effect of agitation on nucleation. There is evidence that fluid shear may increase nucleation by reducing the metastable zone width. However, there is also evidence that too vigorous agitation may hinder nucleation (Liu and Rasmuson, 2013; Mullin and Raven, 1962). In this regard, Liu and Rasmuson measured the induction time of butyl-paraben crystallization in ethanol using small vials (20 ml) equipped with a magnetic stir bar and found that increasing agitation was effective in reducing the induction time only when the stirring rate was below 200 rpm, while more vigorous stirring resulted in a significant increase of the induction time. Therefore, we would expect that using a gentler stirring may actually lead to higher nucleation rate values, similar to those measured for the droplets flowing in the capillary tube. This claim, unfortunately, is only speculative, because it was not possible to lower the stirring speed in the vials to verify this idea, as in the experiments carried out at lower stirring speeds crowning of the crystals on the vial walls occurred (we thus excluded these operating conditions).

5. Conclusions

We estimated the primary nucleation kinetics of para aminobenzoic acid in water in different fluid dynamic conditions using two different experimental devices: a capillary tube where the crystallising solution was held in form of droplets and a set of stirred vials. Due to the small solution volumes used (a few microliters for each droplets and less than a millil-

itre for each vial), we treated nucleation as a stochastic process that can be described by a Poisson distribution. Our results show that by forcing the droplets to move in the capillary tube at constant velocity the nucleation rate increases by two orders of magnitude relative to the rate obtained in stagnant conditions (static droplets). This result confirms the effect of shear rate on the nucleation process. However, the mechanism by which shear rate affects nucleation has not been clearly identified. In this regard, in the literature it has been suggested that shear rate increases the probability of collision of meso-scale clusters in solution, leading to an increase in the rate of crystal formation; at present there is not enough evidence to support this hypothesis in case of PABA crystals.

In *flow conditions*, we observed that the supersaturation ratio does not affect the nucleation rate value, suggesting that the effect of the flow overcomes the effect of supersaturation in the shear rate range analysed. This also confirms the strong effect of shear on the nucleation process.

Finally, we compared these results with those obtained using a commercial stirred multiple reactor system (Crystal16®) at similar supersaturation ratios. We found that although the shear rate achieved in the stirred vials is orders of magnitude larger than the characteristic shear rate in the flowing droplets, the nucleation rates in the capillary system under *flow conditions* are within one order of magnitude of those obtained in the vials, with lower values registered for the vials system. This result suggests that, although shear is effective in enhancing nucleation, increasing the shear rate beyond a certain level may not be beneficial, because it may disrupt the nucleation process. However, further experimental evidence is needed to confirm this hypothesis.

Conflicts of interest

There are no conflicts to declare.

Acknowledgment

Appendix A. Supplementary data

Supplementary data associated with this article can be found, in the online version, at https://doi.org/10.1016/j.cherd.2018.04.039.

References

Castro-Hernández, E., van Hoeve, W., Lohse, D., Gordillo, J.M., 2011. Microbubble generation in a co-flow device operated in a new regime. Lab Chip 11 (12), 2023–2029, http://dx.doi.org/10.1039/c0lc00731e.

Chattopadhyay, S., Erdemir, D., Evans, J.M.B., Ilavsky, J., Amenitsch, H., Segre, C.U., Myerson, A.S., 2005. SAXS study of the nucleation of glycine crystals from a supersaturated solution. Cryst. Growth Des. 5 (2), 523–527, http://dx.doi.org/10.1021/cg0497344.

Coulson, J.M., Richardson, J.F., 1990. Chemical Engineering, vol. 1., 4th ed. Pergamon, Oxford.

Dore, V., Tsaoulidis, D., Angeli, P., 2012. Mixing patterns in water plugs during water/ionic liquid segmented flow in microchannels. Chem. Eng. Sci. 80, 334–341, http://dx.doi.org/10.1016/j.ces.2012.06.030.

Forsyth, C., Burns, I.S., Mulheran, P.A., Sefcik, J., 2016. Scaling of glycine nucleation kinetics with shear rate and glass–liquid interfacial area. Cryst. Growth Des. 16 (1), 136–144, http://dx.doi.org/10.1021/acs.cgd.5b01042.

Forsyth, C., Mulheran, P.A., Forsyth, C., Haw, M.D., Burns, I., Sefcik, J., 2015. Influence of controlled fluid shear on nucleation rates in glycine aqueous solutions. Cryst. Growth Des. 15, 94–102, http://dx.doi.org/10.1021/cg5008878.

Furukawa, H., Kato, Y., Inoue, Y., Kato, T., Tada, Y., Hashimoto, S., 2012. Correlation of power consumption for several kinds of mixing impellers. Int. J. Chem. Eng. 2012, http://dx.doi.org/10.1155/2012/106496.

Galkin, O., Vekilov, P.G., 1999. Direct determination of the nucleation rates of protein crystals. J. Phys. Chem. B 103 (49), 10965–10971, http://dx.doi.org/10.1021/jp992786x.

Gracin, S., Rasmuson, Å.C., 2004. Polymorphism and crystallization of p-aminobenzoic acid. Cryst. Growth Des. 4 (5), 1013–1023, http://dx.doi.org/10.1021/cg049954h.

Gracin, S., Uusi-Penttilä, M., Rasmuson, Å.C., 2005. Influence of ultrasound on the nucleation of polymorphs of p-aminobenzoic acid. Cryst. Growth Des. 5 (5), 1787–1794, http://dx.doi.org/10.1021/cg050056a.

Gray, R.A., Warren, P.B., Chynoweth, S., Michopoulos, Y., Pawley, G.S., 1995. Crystallization of molecular liquids through shear-induced nucleation. Proc. R. Soc. Lond Ser. A: Math. Phys. Sci. 448 (1932), 113 LP-120. Retrieved from http://rspa.royalsocietypublishing.org/content/448/1932/113.abstract.

Hao, H., Barrett, M., Hu, Y., Su, W., Ferguson, S., Wood, B., Glennon, B., 2012. The use of in situ tools to monitor the enantiotropic transformation of p-aminobenzoic acid polymorphs. Org. Process Res. Dev. 16 (1), 35–41, http://dx.doi.org/10.1021/op200141z.

Jawor-Baczynska, A., Moore, B.D., Sefcik, J., 2015. Effect of mixing, concentration and temperature on the formation of mesostructured solutions and their role in the nucleation of DL-valine crystals. Faraday Discuss. 179 (0), 141–154, http://dx.doi.org/10.1039/c4fd00262h.

Jawor-Baczynska, A., Sefcik, J., Moore, B.D., 2013. 250 nm glycine-rich nanodroplets are formed on dissolution of glycine crystals but are too small to provide productive nucleation sites. Cryst. Growth Des. 13 (2), 470–478, http://dx.doi.org/10.1021/cg300150u.

Jiang, S., Ter Horst, J.H., 2011. Crystal nucleation rates from probability distributions of induction times. Cryst. Growth Des. 11 (1), 256–261, http://dx.doi.org/10.1021/cg101213q.

Kurup, G.K., Basu, A.S., 2012. Field-free particle focusing in microfluidic plugs. Biomicrofluidics 6 (2), 1–10, http://dx.doi.org/10.1063/1.3700120.

Laval, P., Crombez, A., Salmon, J.B., 2009. Microfluidic droplet method for nucleation kinetics measurements. Langmuir 25 (3), 1836–1841, http://dx.doi.org/10.1021/la802695r.

Leng, J., Salmon, J.-B., 2009. Microfluidic crystallization. Lab Chip 9 (1), 24–34, http://dx.doi.org/10.1039/b807653g.

Liu, J., Rasmuson, Å.C., 2013. Influence of agitation and fluid shear on primary nucleation in solution. Cryst. Growth Des. 13 (10), 4385–4394, http://dx.doi.org/10.1021/cg4007636.

Liu, J., Svärd, M., Rasmuson, Å.C., 2014. Influence of agitation and fluid shear on nucleation of m-hydroxybenzoic acid polymorphs. Cryst. Growth Des. 14 (11), 5521–5531, http://dx.doi.org/10.1021/cg500698v.

Liu, J., Svärd, M., Rasmuson, Å.C., 2015. Influence of agitation on primary nucleation in stirred tank crystallizers. Cryst. Growth Des. 15 (9), 4177–4184, http://dx.doi.org/10.1021/cg501791q.

Lu, J., Litster, J.D., Nagy, Z.K., 2015. Nucleation studies of active pharmaceutical ingredients in an air-segmented microfluidic drop-based crystallizer. Cryst. Growth Des. 15 (8), 3645–3651, http://dx.doi.org/10.1021/acs.cgd.5b00150.

Mullin, J.W., Raven, K.D., 1962. Influence of mechanical agitation on the nucleation of some aqueous salt solutions. Nature 195, 35–38.

Pan, W., Vekilov, P.G., Lubchenko, V., 2010. Origin of anomalous mesoscopic phases in protein solutions. J. Phys. Chem. B 114 (22), 7620–7630, http://dx.doi.org/10.1021/jp100617w.

Penkova, A., Pan, W., Hodjaoglu, F., Vekilov, P.G., 2006. Nucleation of protein crystals under the influence of solution shear flow. Ann. N. Y. Acad. Sci. 1077, 214–231, http://dx.doi.org/10.1196/annals.1362.048.

Pérez, S.J.A., Porcel, R.E.M., López, C.J.L., Sevilla, F.J.M., Chisti, Y., 2006. Shear rate in stirred tank and bubble column bioreactors. Chem. Eng. J. 124, 1–5, http://dx.doi.org/10.1016/j.cej.2006.07.002.

Poe, S.L., Cummings, M.A., Haaf, M.P., McQuade, D.T., 2006. Solving the clogging problem: precipitate-forming reactions in flow. Angew. Chem. Int. Ed. 45 (10), 1544–1548, http://dx.doi.org/10.1002/anie.200503925.

Rossi, D., Gavriilidis, A., Kuhn, S., Candel, M.A., Jones, A.G., Price, C., Mazzei, L., 2015. Adipic acid primary nucleation kinetics from probability distributions in droplet-based systems under stagnant and flow conditions. Cryst. Growth Des. 15 (4), 1784–1791, http://dx.doi.org/10.1021/cg501836e.

Sullivan, R.A., 2015. Molecules, Clusters and Crystals: The Crystallisation of p-Aminobenzoic Acid from Solution. The University of Manchester.

Sullivan, R.A., Davey, R.J., Sadiq, G., Dent, G., Back, K.R., Ter Horst, J.H., Toroz, D., Hammond, R.B., 2014. Revealing the roles of desolvation and molecular self-assembly in crystal nucleation from solution: benzoic and p-aminobenzoic acids. Cryst. Growth Des. 14 (5), 2689–2696, http://dx.doi.org/10.1021/cg500441g.

Teychené, S., Biscans, B., 2012. Crystal nucleation in a droplet based microfluidic crystallizer. Chem. Eng. Sci. 77, 242–248, http://dx.doi.org/10.1016/j.ces.2012.01.036.

Xiao, Y., Tang, S.K., Hao, H., Davey, R.J., Vetter, T., 2017. Quantifying the inherent uncertainty associated with nucleation rates estimated from induction time data measured in small volumes. Cryst. Growth Des. 17 (5), 2852–2863, http://dx.doi.org/10.1021/acs.cgd.7b00372.